

DARK MATTER DISTRIBUTION IN DISTANT GALAXIES WITH HARMONI

B. Epinat¹, P. Adamczyk¹, S. Bounissou^{1,2}, P. Amram¹ and B. Neichel¹

Abstract.

The study of the distribution of dark matter (DM) in local galaxies has revealed the cusp-core problem. Looking back in time will enable us to understand whether DM halos were already cuspy in the past and evolved with time or if the situation was already similar. We have undertaken HARMONI simulations of galaxies at high redshift from high resolution observations of galaxies in the local Universe to study the potential of HARMONI observations. These simulations show that HARMONI will be able to provide meaningful constraints on DM distribution down to galaxies with stellar masses as low as $10^9 M_{\odot}$ at $z = 1.4$ and that the gain in sensitivity of the 30×60 mas pixel scale is balanced by the better spatial resolution of the 20×20 mas pixel scale to recover the shape of rotation curves.

Keywords: Galaxies: kinematics and dynamics, halos, high-redshift, evolution, dark matter

1 Introduction

The core-cusp discrepancy of dark halo central density distribution between observations and simulations (e.g. Navarro et al. 1997, 2010) remains a challenge for the standard cosmological model. Dynamical processes might be at work to transform cuspy halos into core during galaxy evolution (e.g. Navarro et al. 1996; Teyssier et al. 2013; Ogiya et al. 2014). The dependence of halo concentration with galaxy merger history has been intensively studied from numerical cosmological simulations (e.g. Zhao et al. 2003, 2009). Lambda-CDM numerical simulations like Millennium I-II (Springel et al. 2005; Boylan-Kolchin et al. 2009) indicate that dark halo concentration declines with increasing mass and redshifts (e.g. Bullock et al. 2001). The study of rotation curves enables to constrain dark matter (DM) halo distribution. For this, high resolution kinematics in the inner parts (and ideally neutral gas kinematics beyond the optical disk) are necessary as well as imaging to constrain baryonic mass distribution. Using these techniques Spano et al. (2008) were able to constrain DM distribution for some low mass systems in the local Universe, and suggested that galaxies hosted cored halos. This result was extended to higher masses by Korsaga et al. (2018, 2019). At higher redshift, rotation curves are not yet resolved enough to tackle the cusp-core problem. However, recently, using SINFONI and KMOS data, Genzel et al. (2017) and Lang et al. (2017), tried to constrain the DM fraction in the inner regions of galaxies using both seeing limited and observations assisted with adaptive optics (AO) as well as stacking techniques. Their results points towards a low DM fraction which is supported by the observation of decreasing rotation curves. However, these results remains controversial because the spatial resolution is rather low, the extent of rotation curves is limited and because the seeing may not be properly taken into account. HARMONI on the ELT will be the first instrument able to reach the spatial resolution needed to disentangle the baryonic from the DM distribution for high redshift galaxies. Models of mass distribution will provide constraints on DM halo central density and core radius for galaxies in a redshift range that will remain unreachable with nowadays 8-10 meter class telescopes.

2 Simulations of HARMONI observations: sample selection and description

We have performed a series of simulations to understand the trade off between sensitivity and spatial resolution of kinematics needed to study the DM halo density profiles in distant galaxies. We projected real high resolution

¹ Aix Marseille Univ, CNRS, CNES, LAM, Marseille, France

² CEA Saclay, Service d'Astrophysique, L'Orme des Merisiers, Bat 709, BP 2, 91191 Gif-sur-Yvette Cedex, France

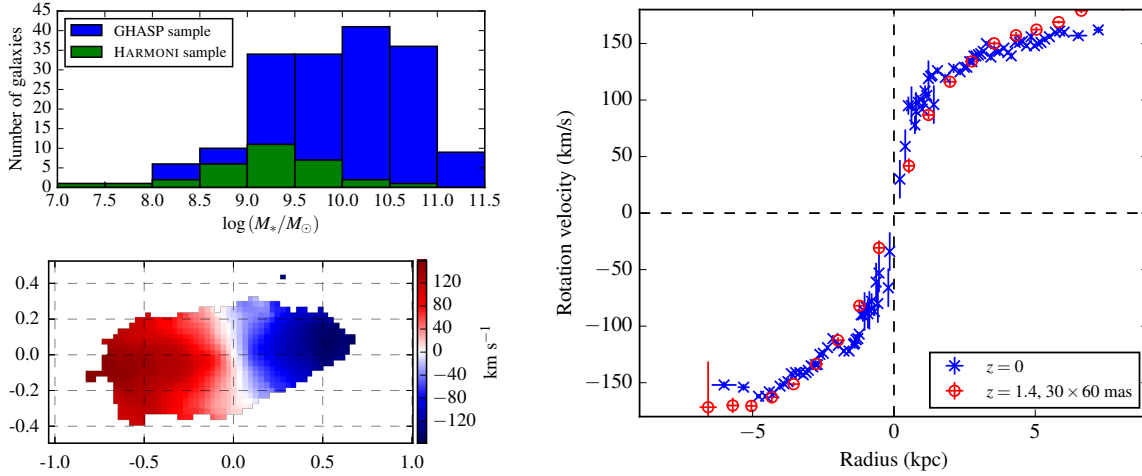


Fig. 1. Top-Left: Stellar mass histogram of both GHASP parent sample (blue) and the HARMONI sub-sample (green). Bottom-left: Velocity field of UGC 7045 with the 30×60 pixel scale. Positions (in arc-seconds) and velocities (km/s) are provided with respect to the adopted centre and systemic velocity of the galaxy respectively. Right: Rotation curve extracted from the velocity field (red). Blue points correspond to the rotation curve obtained at $z = 0$.

Fabry-Perot observations of local galaxies of the GHASP sample (Epinat et al. 2008) at $z = 1.4$, where the angular size is close to the maximal angular distance and where galaxy brightness might be favourable. The GHASP sample consists of 203 spiral galaxies in the local Universe over a large mass range observed using Fabry Perot techniques around the $\text{H}\alpha$ line ($\sim 20 \text{ \AA}$ wide) with a spectral resolution $R \sim 9000$, a spectral sampling of 0.35 \AA and with a spatial resolution of around $3''$ over a field of view of either 4 or 6 arcmin^2 . To ensure that input data cubes have a sufficient spatial resolution to simulate high redshift galaxies, we imposed that the actual physical resolution (FWHM) is larger than the scale corresponding to 20 mas at redshift 1.4, leading to a sub sample of 31 local galaxies. We removed galaxies (i) with ill-defined rotation curves at $z = 0$, (ii) with an inclination larger than 75° , and (iii) with no available stellar mass estimate (from WISE infra-red photometry, Cluver et al. 2014). The HARMONI sub-sample is mainly composed by the low mass galaxies of GHASP (see Fig. 1, top-left). This is due to the fact that high mass galaxies were selected at larger distance to fit within the GHASP field of view and therefore have a lower physical spatial resolutions. Since local galaxies have intrinsic line fluxes much fainter than high redshift ones due to a lower star formation rate (SFR), we have normalised the $\text{H}\alpha$ flux of GHASP galaxies projected at $z = 1.4$ so that all galaxies lie on the Main Sequence of star forming galaxies at $z = 1.4$ using the prescriptions of Whitaker et al. (2014) to convert stellar masses into SFR. The total $\text{H}\alpha$ flux was derived using the Kennicutt (1998) relation using the luminous distance at $z = 1.4$. Assumed SFR range between 10^{-2} and $10^2 M_\odot \text{ yr}^{-1}$ and $\text{H}\alpha$ fluxes between 10^{-19} and $5 \times 10^{-16} \text{ erg s}^{-1} \text{ cm}^{-2}$.

We used these datacubes as input for the HARMONI Simulator (HSIM v1, Zieleniewski et al. 2015). We have generated two sets of pseudo-observations both with a on-source exposure of 2 hours ($8 \times 900 \text{ s}$): one with the 20×20 mas pixel scale and another with the 30×60 mas pixel scale to investigate the trade off between sensitivity (larger with a large pixel), and spatial resolution (better with a small pixel). We used the H-band grism with $R = 7500$ to observe the $\text{H}\alpha$ line at $1.575 \mu\text{m}$ ($z = 1.4$) and a LTAO PSF using 6 laser guide stars under good seeing conditions ($\text{FWHM} = 0.64''$).

3 Simulation analysis

We used CAMEL* (Epinat et al. 2012) on the datacubes produced by HSIM to extract kinematics maps by fitting the spectrum in each spaxel by a Gaussian. For the cubes with the 30×60 mas pixel scale, the data was replicated along the y axis to have a square 30×30 mas final sampling. Prior to kinematics extraction, a 2×2 pixel-wide Gaussian smoothing was applied to increase the signal to noise ratio (SNR). The velocity field was cleaned by removing all spaxels with a SNR below 5 (Fig. 1, bottom-left). The rotation curve (Fig. 1, left) was

*<https://gitlab.lam.fr/bepinat/CAMEL>

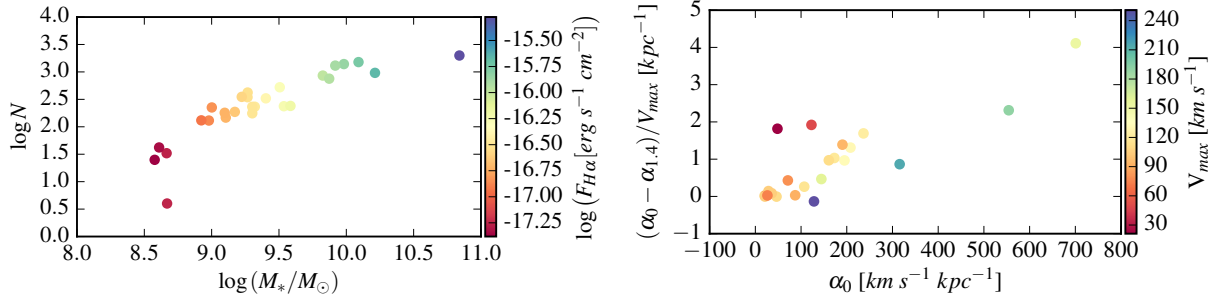


Fig. 2. Left: Number of pixels with a SNR above a threshold of 5 for the 30×60 mas simulations with respect to stellar mass. $H\alpha$ fluxes are indicated using colours. Right: Difference between the slope obtained from high resolution kinematics and HARMONI kinematics using the 30×60 mas simulations, normalised by the maximum rotation velocity as a function of the inner slope from high resolution kinematics. Maximum rotation velocity (from high resolution) is indicated using colours.

then computed using the projection parameters (centre, major axis and inclination) derived from actual data at $z = 0$ by deprojecting off-axis spaxels, as done for local galaxies (e.g. Epinat et al. 2008), within a sector of 30° in the galaxy plane. The point spread function (PSF) was not taken into account. This work therefore represents a lower limit on the capability of HARMONI.

3.1 Signal to noise ratio analysis

Among the 31 galaxies that were simulated, 8 galaxies have less than 100 spaxels with a SNR greater than 5 with both the 20×20 mas and the 30×60 mas pixels scale. These galaxies are those with stellar masses lower than $10^{8.8} M_\odot$ and have integrated fluxes lower than $10^{-17} \text{ erg s}^{-1} \text{ cm}^{-2}$. In Fig. 2 (left), we show the correlation between the number of points have a SNR above 5 and the stellar mass and integrated line flux. From this figure, it is obvious that the most massive galaxies, i.e. those that were not included in the final sub-sample (cf. Fig. 1, top-left) would have a large number of pixels, as expected. Therefore the relatively low number of galaxies with masses above $10^{10} M_\odot$ is not a problem in the present analysis. The observed trend is due to the correlation of size and flux with stellar mass: more massive galaxies have larger number of pixels with good SNR. The 100 pixels threshold corresponds to different area in the galaxies frame depending on the pixel scale. For the 20×20 (30×60) mas pixel scale, this roughly corresponds to 0.04 (0.09) arcsec^2 . The difference observed between the two pixel scales is not very significant and this may be due to the fact that sensitivity gain with the coarser pixel enables to go a bit further. However, it is noticeable that galaxies above the same thresholds in mass and flux are observable under good conditions within the same exposure time with both pixel scales even if surface is slightly larger with the largest pixel. In some cases, the 20×20 mas pixel scale even provides a better detection because emission is clumpy, hence the SNR is better because clumps are not resolved. For the lowest mass galaxies, except in specific cases, the gain in sensitivity using the coarser pixel is not sufficient to compensate the intrinsically small size of galaxies. It is remarkable that in 2 observing hours we are able to spatially resolve galaxies down to masses of $10^9 M_\odot$ at $z = 1.4$, which is very challenging with actual telescopes in tens of hours (e.g. Contini et al. 2016; Newman et al. 2012).

3.2 Rotation curve analysis

With actual telescopes without AO, the maximum rotation velocity can already be quite efficiently recovered. However, it is almost impossible to constrain the inner slope which contains information about a cuspy or core DM halo. The visual inspection of rotation curves for our sub-sample is promising (cf. Fig. 1, right). For all galaxies that passed the selection threshold on SNR, the derived rotation curves have a fairly good overall agreement for both the 30×60 and 20×20 pixel scales. There are two exceptions, the two faintest galaxies, where the rotation curve obtained with the 30×60 mas scale looks better. The 20×20 mas rotation curve shows more resolved details than the 30×60 mas one. In addition, the inner slope seems better resolved. The inner velocity gradient is usually well recovered, even if it seems slightly underestimated.

We further quantified the recovery of the inner velocity gradient from the rotation curve. We have estimated

the inner gradient within the inner 500 pc of each galaxy on both the 20×20 mas and 30×60 mas pixel scales. We compared these values to inner slopes that were estimated from the high resolution data in Epinat et al. (2010). Fig. 2 (right) shows the inner slope difference between $z = 0$ data and projected data, normalised by the maximum velocity inferred at $z = 0$ as a function of the $z = 0$ inner slope. We observe a trend that the normalised slope difference is larger when the inner gradient is large. For a given inner slope, the normalised difference is lower for the fastest rotators. The inner slopes are also better recovered with the smallest pixel scale, even if the difference is not strong. For the slow rotators, the difference is larger with the small pixel scale, probably because these galaxies are the lowest mass galaxies, and hence have a lower SNR, preventing accurate velocity measurements.

4 Conclusions

We have performed analysis of advanced HSIM simulations of local galaxies projected at redshift $z=1.4$ and have found that: (i) HARMONI will be able to study spatially resolved kinematics with sufficient details and signal to noise ratio to perform mass models and recover the shape of DM halos down to stellar masses of $10^9 M_{\odot}$ at $z = 1.4$ and $10^{9.5} M_{\odot}$ at $z = 2.7$ using the H α line in 2 hours of exposure. This translates into a line flux limit of 10^{-17} erg s $^{-1}$ cm $^{-2}$ and can be at first approximation applied for any other emission line. (ii) The gain in sensitivity of the coarser pixel scale (30×60 mas) enables to go slightly deeper than the 20×20 mas pixel scale. (iii) This gain in sensitivity is balanced by the lower spatial resolution of the 30×60 mas pixel scale. The 20×20 mas pixel scale enables to better recover the details and shape of the rotation curve.

Mass models will need methods taking into account beam smearing. In addition, in this study, we did not recover projection parameters (PA, inclination and centre) from the data. These parameters might be either recovered from kinematics, using 2D or 3D modelling techniques or using continuum emission. In order to perform mass model analyses one also needs to know stellar and gas distributions. We will investigate whether HARMONI data will enable to perform photometry and morphology analyses or if ancillary data are necessary.

Studying the capabilities of ELT-MOS on this topic is of major importance to assemble a statistical sample.

This work is supported by CNRS/INSU, with funding from CSAA, ASHRA, PNCG.

References

- Boylan-Kolchin, M., Springel, V., White, S. D. M., Jenkins, A., & Lemson, G. 2009, MNRAS, 398, 1150
 Bullock, J. S., Kolatt, T. S., Sigad, Y., et al. 2001, MNRAS, 321, 559
 Cluver, M. E., Jarrett, T. H., Hopkins, A. M., et al. 2014, ApJ, 782, 90
 Contini, T., Epinat, B., Bouché, N., et al. 2016, A&A, 591, A49
 Epinat, B., Amram, P., Balkowski, C., & Marcelin, M. 2010, MNRAS, 401, 2113
 Epinat, B., Amram, P., Marcelin, M., et al. 2008, MNRAS, 388, 500
 Epinat, B., Tasca, L., Amram, P., et al. 2012, A&A, 539, A92
 Genzel, R., Schreiber, N. M. F., Übler, H., et al. 2017, Nature, 543, 397
 Kennicutt, Robert C., J. 1998, ApJ, 498, 541
 Korsaga, M., Amram, P., Carignan, C., & Epinat, B. 2019, MNRAS, 482, 154
 Korsaga, M., Carignan, C., Amram, P., Epinat, B., & Jarrett, T. H. 2018, MNRAS, 478, 50
 Lang, P., Förster Schreiber, N. M., Genzel, R., et al. 2017, ApJ, 840, 92
 Navarro, J. F., Frenk, C. S., & White, S. D. M. 1996, ApJ, 462, 563
 Navarro, J. F., Frenk, C. S., & White, S. D. M. 1997, ApJ, 490, 493
 Navarro, J. F., Ludlow, A., Springel, V., et al. 2010, MNRAS, 402, 21
 Newman, S. F., Genzel, R., Förster-Schreiber, N. M., et al. 2012, ApJ, 761, 43
 Ogiya, G., Mori, M., Ishiyama, T., & Burkert, A. 2014, MNRAS, 440, L71
 Spano, M., Marcelin, M., Amram, P., et al. 2008, MNRAS, 383, 297
 Springel, V., White, S. D. M., Jenkins, A., et al. 2005, Nature, 435, 629
 Teyssier, R., Pontzen, A., Dubois, Y., & Read, J. I. 2013, MNRAS, 429, 3068
 Whitaker, K. E., Franx, M., Leja, J., et al. 2014, ApJ, 795, 104
 Zhao, D. H., Jing, Y. P., Mo, H. J., & Börner, G. 2009, ApJ, 707, 354
 Zhao, D. H., Mo, H. J., Jing, Y. P., & Börner, G. 2003, MNRAS, 339, 12
 Zieleniewski, S., Thatte, N., Kendrew, S., et al. 2015, MNRAS, 453, 3754